AMERICAN METEOROLOGICAL SOCIETY

Journal of Applied Meteorology and Climatology

EARLY ONLINE RELEASE

The DOI for this manuscript is doi: 10.1175/JAMC-D-16-0393.1

Recent changes in United States regional heat wave characteristics in observations and reanalyses

J.T. Schoof[*1], T.W. Ford[1], S.C. Pryor[2]

[1]Department of Geography and Environmental Resources,
Southern Illinois University, Carbondale, IL, USA

[2]Department of Earth and Atmospheric Sciences,
Cornell University, Ithaca, NY, USA

Revision submitted to Journal of Applied Meteorology and Climatology
July 2017

*Corresponding author address: J.T. Schoof, Department of Geography and Environmental Resources, Southern Illinois University, MC 4514, 1000 Faner Dr., Carbondale, IL 62901
E-mail: jschoof@siu.edu, Tel: (618) 453-6019

Abstract

Humidity is a key determinant of heat wave impacts, but studies investigating changes in extreme heat events have not differentiated between events characterized by high temperatures and those characterized by simultaneously elevated temperature and humidity. We present a framework, using air temperature (T) and equivalent temperature (T_E; a measure combining temperature and specific humidity), to examine changes in local percentile-based extreme heat events characterized by high temperature (T-only) and those with high temperature and humidity (T-and-T_E events). Application to one observational data set (PRISM), four reanalysis products (1981-2015) and seven U.S. regions reveals widespread changes in heat wave characteristics over the 35-year period. Agreement among the data sets employed on several heat wave metrics suggests that many of the findings are robust. With the exception of the Northern Plains region, all regions experienced increases in both T-only and T-and-T_E heat wave day (HWD) frequency in each of the reanalyses. In the Northern Plains, all data sets have negative trends in T-only HWD frequency and positive trends in T-and-T_E HWD frequency. Trends in HWD frequency were generally accompanied by changes in the spatial footprint in heat wave conditions. Finally, temperature has increased significantly during T-only HWDs in the western regions, while increases in T_E during T-and-T_E HWDs have occurred in the central US and Northeast region. Our findings suggest that equivalent temperature provides an alternative perspective on the evolution of regional heat wave climatology. Studies considering changes in regional heat wave impacts should carefully consider the role of atmospheric moisture.

1. Introduction

Extreme heat is associated with impacts across a range of sectors, including agriculture (Lobell et al., 2014), energy use (Miller et al., 2008), and human health (Anderson and Bell, 2011). Despite the presence of air conditioning in more than 90% of U.S. homes (Davis and Gertler, 2015), in most years extreme heat remains the largest cause of weather-related mortality in the U.S. (NWS, 2016). Near-surface humidity is a key determinant of impacts associated with extreme temperatures, with high humidity heat waves leading to elevated morbidity/mortality in people (Kravchenko et al., 2013) and prolonged periods of high temperatures and low humidity associated with precipitation deficits (i.e., meteorological droughts) leading to reduced agricultural yields (Mishra and Cherkauer, 2010). Given historical increases in temperature extremes (Seneviratne et al., 2014) and specific humidity (Dai, 2006) and robust projections of future temperature increases (Collins et al., 2013) and associated changes in column-integrated water vapor (Held and Soden, 2006), there is a need to better understand changes in the moisture content of heat waves.

The combined effects of temperature and humidity have been considered in several previous studies through application of apparent temperature (T_a; Steadman, 1984), most commonly using the simplified formula that ignores the effects of wind and radiation:

$$T_a = -1.3 + 0.92T + 2.2e \quad (1)$$

where T is the air temperature (°C) and e is the vapor pressure (kPa). Gaffen and Ross (1998) found a significant increase in T_a heat waves during 1949-1995 with the strongest signal in the western U.S. More recently, Grundstein and Dowd (2011) reported acceleration of those trends and also noted an increase in the frequency of days with extreme values of T_a. While the utility of T_a for studying heat-related morbidity and mortality has been demonstrated (e.g., Metzger et

68 al., 2010), high values of T_a are possible in the absence of high humidity, given sufficiently high
69 air temperature. For the purpose of differentiating between high and low humidity extreme
70 events, we adopt equivalent temperature (T_E; °C) which is given by:

71 $$T_E = T + \frac{L_v q}{C_p} \quad (2)$$

72 where T is the air temperature (°C), L_v is the latent heat of vaporization (J kg^{-1}), q is the specific
73 humidity (kg kg^{-1}) and C_p is the specific heat of air at constant pressure (1005 J kg $°C^{-1}$).
74 Relative to T_a, T_E is much more responsive to changes in humidity (Pielke et al., 2004). For
75 example, at 35°C, a 1°C increase in the dew point temperature from 19°C to 20°C, raises T_a by
76 0.31°C, but raises T_E by 2.15°C. The upper tail of the T_E distribution is therefore comprised only
77 of events characterized by high temperature and high humidity. Previous analyses have
78 identified larger variability and stronger trends in T_E, relative to T, particularly during summer as
79 a result of increasing specific humidity (e.g., Davey et al., (2006); Fall et al., (2010), Schoof et
80 al., (2015)). Conceptually, variations in T_E might result from (1) global or hemispheric changes
81 in specific humidity accompanying large scale warming, (2) changes in circulation that govern
82 regional moisture transport (Ford and Schoof 2016), and/or (3) changes in local forcing related to
83 local land cover, soil moisture variations (including those deriving from irrigation, Pryor et al.
84 (2016)), and land-atmosphere interaction (Ford and Schoof (2017); Pryor and Schoof (2016)).
85 T_E is thus ideal for differentiating between T-only heat wave conditions (T is elevated, but T_E
86 is not) and T-and-T_E heat wave conditions (both T and T_E are elevated) in climatic time series.
87 The former represent hot and dry extremes while the latter represent hot and moist extremes.
88 Here, we use this framework to characterize changes in heat wave day characteristics for U.S.
89 regions (Figure 1). We adopt the regional delineation used by the recent U.S. National Climate
90 Assessment (Melillo et al., 2014), but follow Bosilovich (2013) and further subdivide the Great

Plains region into southern and northern regions to account for differences in hydroclimatology across the central U.S. Each of the regions is also characterized by sub-regional variability resulting from variations in topography, land cover, and other factors. Here, we are primarily interested in broad regional changes, but where appropriate, we note instances where changes are sub-regional in nature. Similar regional definitions have been adopted in previous studies of regional temperature and humidity (e.g., Gaffen and Ross, 1999; Brown and DeGaetano 2013). Our investigation is based on results derived from high resolution quality controlled observational reference data (PRISM; Daly et al. 2008) and retrospective analysis ("reanalysis") data. The data are described in Section 2. In Section 3, we describe the metrics used in our trend analysis. The results are presented in Section 4 and summarized in Section 5.

2. Data

Air temperature and humidity time series from surface stations suffer from inhomogeneities associated with station moves, sensor changes, urbanization and other factors. These changes sometimes require time series adjustments, such as those applied in Brown and DeGaetano (2013) before temporal trends can be assessed. Given our focus on regional analyses, and the strong effects of local land cover (Fall et al. 2010), and irrigation (Pryor et al. 2016), on temperature and humidity, we opt to use (1) the PRISM gridded temperature and dew point temperature products (Daly et al. 2008) which are highly quality controlled and spatially and serially complete and (2) reanalysis data, which integrate observational data and numerical models to produce temporally and spatially consistent outputs (Bosilovich, 2013).

2.1. Reanalysis data

114 Four reanalysis products (Table 1) are considered in this study: the European Center for
115 Medium-Range Weather Forecasts (ECMWF) Interim Reanalysis (ERA-Interim; Dee et al.,
116 2011), the Japanese Meteorological Agency (JMA) 55-year Reanalysis (JRA-55; Kobayashi et
117 al., 2015), the National Aeronautical and Space Administration (NASA) Modern Era
118 Retrospective Analysis for Research and Applications 2 (MERRA-2; Bosilovich et al., 2015),
119 and the National Centers for Environmental Prediction (NCEP) North American Regional
120 Reanalysis (NARR; Mesinger et al., 2006). These reanalyses were chosen because they span a
121 range of spatial resolutions (32 km for NARR up to 1.25° for JRA-55), are continuously updated,
122 and vary in terms of assimilated variables. Both ERA-Interim and JRA-55 assimilate near
123 surface temperature and humidity data from surface stations. MERRA-2 does not assimilate 2-m
124 temperature or humidity over land (Bosilovich, personal communication), while NARR
125 assimilates near surface humidity, but not temperature. In an assessment of several reanalyses,
126 including ERA-Interim, NARR, and earlier versions of JMA (JRA-25) and NASA (MERRA)
127 reanalyses, Vose et al., (2012) found that the reanalysis-derived temperature trends for the
128 contiguous United States (1979-2008) bracket those derived from an adjusted station network
129 (USHCN). Bosilovich (2013) compared summer temperature and precipitation variations in
130 several reanalyses to observations and found that variability and trends in temperature were more
131 similar than those for precipitation. In Section 3, we assess multiple aspects of reanalysis
132 performance relative to gridded, quality controlled observations.
133
134 *2.2. Observational data*
135 Prior to using reanalysis data to estimate changes in the heat wave characteristics, we first
136 assess the spatio-temporal variability of reanalysis-derived 2-m temperature, specific humidity,

and equivalent temperature series with those from PRISM. Here, we use daily temperature and dew point temperature from PRISM with a resolution of 2.5 arc-minutes (approximately 4km). PRISM, described more fully in Daly et al. (2008), combines station observations from multiple networks with a digital elevation model to provide gridded data for the contiguous United States. It has been widely used in applied climatological settings.

3. Methods

The ERA-Interim and JRA-55 output is available at 6-h increments, while NARR data are available at 3-h increments and MERRA-2 data are available at hourly resolution. For consistency, we sampled all products every 6-h at 0, 6, 12, and 18 GMT and then computed daily averages. The JRA-55, MERRA-2, and NARR products included 2-m temperature and specific humidity in their output. The ERA-Interim output does not include near-surface specific humidity, so it was calculated from 2-m dew point temperature and surface pressure using:

$$e = 6.112 \exp\left(\frac{17.67T_d}{T_d+243.5}\right) \quad (3a)$$

$$q = \frac{0.622e}{P-0.378e} \quad (3b)$$

where T_d is the dew point temperature (°C), e is the vapor pressure (hPa), P is the surface pressure (hPa) and q is the specific humidity (kg kg^{-1}) (Bolton 1980). The observational data (PRISM) also consist of 2-m temperature and 2-m dew point temperature. We therefore used the pressure field from the highest resolution reanalysis product (NARR) to compute q, again using Equations 3a and 3b. Since the observed pressure field is assimilated by all the reanalyses, the resulting q field is not sensitive to the choice of NARR for this purpose.

3.1. Assessment of reanalyses relative to PRISM and each other

160 To assess the spatio-temporal variability of reanalysis-derived 2-m temperature (T), specific
161 humidity (q) and equivalent temperature (T_E) relative to PRISM, we computed (1) the mean and
162 standard deviation of the summer (JJA) daily values, (2) the interannual variability of the JJA
163 means, defined as the standard deviation of the 1981-2015 (n=35) values, and (3) the linear trend
164 of the JJA means. Because the reanalyses differ in terms of spatial resolution (Section 2.1), each
165 metric was computed at the native reanalysis resolution and then interpolated to the PRISM grid
166 covering the contiguous United States using bilinear interpolation. For each metric, we develop
167 a Taylor diagram (Taylor, 2001) that displays the pattern correlation between PRISM and each
168 reanalysis product, the standard deviation of the spatial fields from PRISM and each reanalysis
169 product and the pattern-centered root mean square error between PRISM and each reanalysis
170 product. Pattern-centered statistics, such as those employed in Taylor diagrams, are designed to
171 compare spatial patterns, but do not aid in identification of regional biases. We therefore
172 supplement our analysis of patterns with regional averages of each metric. This combination
173 allows us to simultaneously assess the reanalyses in terms of their spatial patterns and regional
174 biases with respect to multiple descriptors of T, q, and T_E.
175
176 *3.2. Heat wave definitions*
177 Although heat waves are commonly understood to be time periods with near surface air
178 temperatures that are well above average, there is no universally accepted definition of a heat
179 wave (Souch and Grimmond, 2004). Given the clear evidence for acclimatization to heat
180 extremes (Hondula et al. 2015), we use locally derived percentile-based thresholds rather than
181 absolute thresholds. Specifically, we use a 15-day moving window centered on each JJA
182 calendar day to define a 90^{th} percentile daily values for T and T_E, using data from 1981-2015. A

183 day is a heat wave day if both the daily temperature and the three-day average temperature (i.e.,
184 the mean of the current day and the previous two days) exceed the 90th percentile daily value. If
185 the current day has a value of T_E that falls below the 90th percentile T_E value, the current day is
186 considered to be a T-only heat wave day. Conversely, if the current day has a value of T_E that
187 exceeds the 90th percentile T_E value, the current day is considered to be a T-and-T_E heat wave
188 day.

189 Using the definitions above for T-only and T-and-T_E heat wave days, we compute several
190 metrics of heat wave frequency and magnitude for each summer between 1981 and 2015. To
191 characterize heat wave day frequency, we consider the mean (over each region) number of JJA
192 heat wave days (HWDs) for T-only and T-and-T_E type heat waves. Assessing changes in heat
193 wave day magnitude (i.e., intensity) requires a different approach since extreme heat events have
194 both a spatial footprint and a magnitude. To address this issue, for each day (n=3220; 92 days
195 per summer × 35 summers) we compute the spatial proportion [0,1] of each region impacted by
196 each type of heat wave event as well as the event magnitude, defined as the average departure
197 from the heat wave day threshold (90th percentile as defined above) among grid points
198 experiencing heat wave conditions. We then consider the mean and maximum values of the
199 spatial proportion and mean magnitude for each summer.

200 To synthesize our results, we compute each heat wave day characteristic at the native data
201 resolution (see Section 2), but report values for the regions in Figure 1. Due to short time series
202 and high interannual variability in heat wave frequency, trend analysis was conducted on each of
203 the heat wave day metrics using the nonparametric Theil-Sen estimator (Sen 1968) also known
204 as median-of-pairwise-slopes regression (Lanzante 1996).
205

4. Results

4.1. Assessment of reanalysis products

Each of the reanalysis products considered in this study reproduces the mean and standard deviation of 2-m T, q, and T_E (Figures 2-4). Comparison of the maps of mean T and mean T_E (cf., Figure 2a and Figure 4a) highlights important differences between these variables. Air temperatures are highest in the desert SW and throughout the SP and SE regions (Figure 2a), while T_E is highest in the warm and humid climate of the SE region as a result of the influence of near-surface humidity which exhibits a strong contrast between the humid SE region and the dry western regions (Figure 3a). Variability of daily T is negatively correlated with the mean over space, while the variability of daily q is highest in the monsoon region of the SW (Figure 3b). Variability of daily T_E (Figure 4b) exhibits a pattern more like that of q than T. Correlations between PRISM and reanalysis derived fields of the mean and standard deviation of daily T, q, and T_E generally exceed 0.9 (Figures 2a, 2b, 3a, 3b, 4a, and 4b) indicating strong agreement among observations and reanalyses for these basic climate descriptors. While the regional means derived from the reanalysis generally bracket the estimate derived from PRISM, each of the reanalyses are slightly warmer on average than PRISM in the NP region (Figure 2i) and NARR exhibits a warm bias across most regions relative to PRISM and the other reanalyses. The reanalyses are also more variable than PRISM for T, q, and T_E across most regions (Figure 2j, 3j, and 4j).

Since heat waves exhibit substantial variability from one summer to the next, assessment of interannual T, q, and T_E variability in observations and reanalysis is an important step toward understanding differences in their heat wave climatologies. Correlations between PRISM and reanalysis-derived fields of interannual variability range from 0.74 to 0.84, 0.65 to 0.75 and 0.85

229 to 0.95 for T, q, and T_E, respectively (Figure 2g, 3g, 4g). The reanalyses therefore agree with
230 PRISM with respect to the spatial pattern of interannual variability. Examination of regional
231 values of interannual temperature variability indicates that MERRA-2 is biased high relative to
232 PRISM and other reanalyses across the eastern and central US (Figure 2k). MERRA-2 and
233 NARR also exhibit some regional biases in interannual variability of q (Figure 3k).
234 PRISM and reanalysis-derived trends of T, q, and T_E show qualitative similarity, but some
235 notable regional differences (Figures 2-4). Apart from the SE region, the T trends vary
236 substantially within US regions. For example, NARR shows much less warming than PRISM or
237 the other reanalyses in the western US (Figure 2l) and all of the reanalyses exhibit more warming
238 than PRISM in the SE, MW, and SP regions. Despite the small-scale cooling across parts of the
239 NP and MW regions (which is reproduced to varying degrees in the reanalyses), the 35-yr linear
240 trends in temperature are positive across all regions and data sets. Temperature trends derived
241 from PRISM are significant (α=0.10) in the NE, SE, SP, SW, and NW regions. All of the
242 reanalysis-derived temperature trends are significant in the SE, SP, and SW regions and none of
243 the reanalyses indicate significant warming the MW or NP. The warming pattern in NARR
244 (warm faster than other data products in the east and slower than other data products in west)
245 results in a low pattern correlation between PRISM and NARR-derived temperature trends.
246 Unlike the temperature trends presented in Figure 2, the humidity trends (Figure 3d) differ in
247 sign among regions and in some cases among reanalyses within a region (Figure 3l). MERRA-2
248 stands out in this analysis as the only product with positive near-surface specific humidity trends
249 in all US regions, including the SW, where warming and drying have been well documented
250 (e.g., MacDonald, 2010). Observed (PRISM) humidity trends are large and positive in the NP
251 and NE regions, but are positive throughout most of the eastern US. Conversely, the SW and

NW regions are characterized by negative humidity trends in PRISM. In all regions, the reanalysis-derived q trends bracket the PRISM-derived regional trends. The trend toward increasing near-surface humidity is significant (α=0.10) in the NE region in PRISM and in all of the reanalyses. Only ERA-Interim and NARR produce a significant downward trend in q in the SW region. In the JRA-55 and MERRA-2 reanalyses, the upward trend in q is significant.

Since T_E is dependent on both T and q (Eq. 2), temporal trends in T_E depend on the underlying temperature and humidity trends. Because NARR (T) and MERRA-2 (q) did not adequately reproduce the spatial patterns of the latter, the pattern correlations between PRISM and reanalysis-derived T_E trends for those products are relatively low, although it should be noted that the other reanalyses (ERA-Interim and JRA-55) only correlate spatially with PRISM at around 0.5. Nonetheless, the regional values of the T_E trends derived from ERA-Interim and JRA-55 show stronger agreement with PRISM (Figure 4l). The largest linear trends in T_E are found in the NE region, where the positive trends are significant in PRISM as well as three of the four reanalyses. Small increases in temperature, coupled with large increases in humidity resulted in a significant trend in the NP region in PRISM. With the exception of the SW, the reanalyses agree with PRISM in terms of the sign of the T_E trend, but there are substantial differences among the data products in terms of the trend magnitude.

The analyses presented thus far demonstrate that (1) no single reanalysis product is optimal in terms of all of the metrics considered and (2) temperature and equivalent temperature differ in terms of both their general statistical characteristics and temporal trends. Consistent with *a priori* expectations that assimilation of station T and q will improve depiction of weather and climate in reanalyses (Bosilovich 2013), our results indicate generally superior performance of ERA-Interim and JRA-55 with respect to temporal variability and trends, although there are

instances where these products perform less well than MERRA-2 and NARR. Because the reanalyses exhibit individual strengths and weaknesses relative to observations, our analysis of heat wave characteristics is conducted with all the products and we use the results presented in this section to contextualize our findings related to changes in heat wave characteristics.

4.2. Historical changes in heat wave characteristics

4.2.1. Heat wave day (HWD) frequency

The heat wave day (HWD) definition adopted in this study is based on the 90th percentile of T (Section 3.2). However, the requirement that the 3-day average T exceeds the 90th percentile results in substantially fewer than 10% of summer days meeting the criteria. Based on the PRISM data set, the regions in Figure 1 experience an average of 4.4 (NP) to 5.5 (SP) HWDs per summer, but the partitioning of days between T-only and T-and-T_E HWDs differs among the regions (Figure 5a,b), and all regions exhibits substantial interannual variability in HWD frequency (Figure 6). For example, T-only HWDs comprise more than 80% of all HWDs in the SP region, but only around 20% of the HWDs in the NE region (Figure 5a, b).

Because the heat-wave definition adopted here requires multiple days above the 90th percentile value, persistence of daily temperature is a key characteristic of reanalysis data in the context of T-only HWD frequency. Reanalyses with high persistence in daily T, as characterized by the lag-1 Spearman correlation, generally have higher regional mean HWD counts. Considering each region and data product as a data point (n=35), the correlation between the lag-1 correlation of T and regional mean HWD frequency is 0.57 ($p<0.01$). Similarly, the partitioning of HWDs among T-only and T-and-T_E HWDs exhibits dependence on the coupling of T and q, as characterized by the Spearman correlation between their daily means. Figure 7a

298 shows the frequency of T-and-T_E HWDs as a function of the correlation between daily mean T
299 and q and demonstrates that tighter coupling between daily T and q is associated with a higher
300 proportion of heat waves characterized by high temperature and high humidity (i.e., T-and-T_E
301 HWDs). In general, there is closer accord in both frequency of HWDs and partitioning of HWDs
302 in those reanalyses that assimilate near surface T and/or q (JRA-55, ERA-Interim and NARR),
303 while MERRA-2 tends to overestimate T-only HWD frequency and underestimate T-and-T_E
304 HWD frequency in the western and central US regions.

305 The time series of regional HWD frequencies (Figure 6) also highlight the utility of our
306 framework for identifying regional variations in the partitioning of HWDs between T-only and
307 T-and-T_E varieties as well as important historical events. Note, for example, the high number of
308 T-and-T_E HWDs, and relatively few T-only HWDs in the MW region during the summer of 1995
309 (Figure 6c), which led to major loss of life in Chicago and surrounding areas (Kunkel et al.,
310 1996). Conversely, the summer of 1988 was characterized by a much larger number of total heat
311 waves, with similar numbers of T-only and T-and-T_E HWDs, in the central US regions,
312 consistent with the widespread North American drought of that summer (Trenberth and
313 Branstator, 1992). The 2011 heat wave (Hoerling et al., 2013) was also associated with drought
314 conditions and produced record numbers of HWDs, nearly all T-only, in the SP region (Figure
315 6e).

316 Trend analyses conducted on the time series in Figure 6 (and similar series in the reanalyses
317 products) result in identification of several significant trends and many trends that, while not
318 statistically significant, are of consistent sign among the data sets employed (Table 2). With the
319 exception of the NP region, which is characterized by non-significant decreases in all of the data
320 products, all regions are characterized by positive trends in T-only HWDs in PRISM and the four

reanalyses tested. The largest increases in T-only HWDs have occurred in the SP and SW regions, where the trends are statistically significant (α=0.10) in all of the data sets (Table 2). The T-only HWD trends are also significant in the NW region for PRISM, ERA-Interim, and JRA-55 and in the SE for ERA-Interim and JRA-55. While the magnitude of the trends vary within regions, the PRISM- and reanalysis-derived trends show good qualitative agreement. Similarly, PRISM and all of the reanalyses produce positive trends in T-and-T_E HWD frequency in all of the CONUS regions. The largest trends (Table 2) are in the NE, NW, and MW regions and despite large interannual variability in T-and-T_E HWD frequency, the trends are statistically significant in some of the data sets (MERRA-2 and NARR for the NE and MW regions, ERA-Interim and JRA-55 for the NW). The SP region is characterized by smaller trends, but given less variability in the time series, the trends are significant in all of the products tested (Table 2).

4.2.2. Spatial extent of heat wave conditions

The changes in heat wave day frequency presented in Section 4.2.1 may be manifest as more or less spatially extensive heat waves. We therefore computed the spatial proportion of each region impacted by each type of heat wave event for each summer day from 1981-2015. For each summer, we then computed the mean and maximum proportions over all days for which the proportion was greater than zero. The resulting time series for the mean spatial proportion (from PRISM) are shown in Figure 8 and linear trends in the mean and maximum spatial proportion from all data products are presented in Table 3.

The largest trends in the mean spatial proportion of T-only HWDs correspond to the regions with significant trends in T-only HWD frequency presented in Table 2 and Figure 6. Specifically, the SP, SW and NW regions exhibit positive trends in all of the data products with

significant trends in PRISM, ERA-Interim, and JRA-55. As with the T-only HWD frequency, the NP region is characterized by (insignificant) decreases in T-only HWD areal proportion in all of the data products. In regions characterized by increases in the mean areal proportion impacted by T-only heat wave conditions, the maximum areal proportion impacted by T-only HWDs has also increased, and has done so at a much faster rate than reported for the mean (Table 3). All of the data products tested produce significant positive trends in the maximum summer proportion of the SP and SW regions impacted by T-only heat wave conditions (Table 3).

Trends in the mean regional proportion impacted by T-and-T_E heat wave conditions are positive in all data products for the SE, SP, and NW regions, but lack strong agreement among the reanalyses with respect to the magnitude and statistical significance of the trend. In other regions, the trends in regional proportion derived from different data sets span zero indicating uncertainty in the temporal evolution of the average footprint of T-and-T_E heat wave conditions. There is less ambiguity in the maximum spatial proportion of T-and-T_E heat wave conditions, which exhibit positive trends across data products in all regions except the NP. In other regions, PRISM and all four reanalysis products are characterized by positive trends in the maximum regional proportion impacted by T-and-T_E heat waves, with significant trends in some but not all reanalyses.

4.2.3. Heat wave day (HWD) magnitude

Even though the percentiles used in our heat wave definition are location specific, there are still important regional variations in heat wave magnitude (Figure 5). For T-only HWDs, the average T magnitude in the PRISM data set ranges from around 0.9°C in the SE region to around 1.6°C in the NP region. Values derived from the reanalyses are generally slightly higher (Figure

5c). In most regions, temperatures are lower on T-only HWDs relative to T-and-T_E HWDs, which also exhibit greater variability between regions (cf. Figure 5c and 5d). Overall, the reanalyses show agreement with each other and with PRISM with respect to average temperature characteristics of T-and-T_E heat waves. The magnitude of T_E during T-and-T_E heat waves is likewise characterized by strong regional variations, but good agreement among PRISM and the reanalyses. Variations among regions are intuitive; the SW and SP regions tend to have dry heat waves relative to other regions, resulting in lower T_E magnitude across HWD types. Regional differences in T_E magnitude on T-and-T_E HWDs, and in some cases, variations among reanalysis products within regions, are highly correlated ($r=0.84$, $p<0.01$) with the correlation between daily T and q (Figure 7b) with greater T_E magnitudes associated with stronger coupling of T and q.

To assess trends in the magnitude of T and T_E on HWDs, we computed the mean magnitude (difference between the daily T or T_E and the 90th percentile threshold) for each day at locations with positive (i.e., heat wave) values. We then computed the average and maximum value over each summer to produce time series (Figure 9). In the western regions (SW, NW), where the background warming has been greatest, there has been an increase in the magnitude of T on T-only HWDs. This trend is positive across data sets in both regions and significantly positive in the PRISM and JRA-55 products (Table 4). The SE region is also characterized by trends that are positive across data products, but not large enough to be considered statistically significant. In other regions, the data products produce a mixture of positive and negative trends, leading to greater uncertainty in the evolution of the magnitude of temperature during T-only heat wave events. The reanalyses show similarly small trends of mixed sign for T magnitude during T-and-T_E heat waves (Table 4).

Trends in the magnitude of T_E during T-and-T_E heat waves show greater similarity among the data sets (Table 4). In the PRISM data set, the trends are significant for the MW and NP regions. While not all of the reanalyses produce significant trends, they are all positive in agreement with PRISM. Positive trends are also observed in all data products in the NE region, with significant trends in the MERRA-2 and NARR products. The SW region is characterized by declining T_E during T-and-T_E heat wave events (significantly in the ERA-Interim and JRA-55 reanalyses), consistent with the general drying trend observed in that region.

Trends in maximum T magnitude on T-only HWDs show consistent (among the data sets) and significant (in PRISM and at least one reanalysis) increases in the SE and NW regions over the period 1981-2015 (Table 3). In other regions, there are variations in the sign of the trend among data products. Trends in maximum T magnitude on T-and-T_E HWDs are likewise variable among the reanalyses and are only of consistent sign in the NE region, where the PRISM trend is significant (α=0.1). Trends in maximum T_E magnitude on T-and-T_E HWDs are more consistent among the data products with increases in the NE, NP, and SP regions across data sets.

5. Summary and Conclusions

We have conducted the first analysis of United States regional heat wave characteristics using T and T_E and compared time series of PRISM- and reanalysis-derived temperature (T) and equivalent temperature (T_E) to investigate recent historical changes in heat wave characteristics. Our results show that heat wave days (HWDs) are generally becoming more frequent and more spatially expansive, consistent with increases in summer air temperature. With the exception of the NP region, where T-only HWD frequency has declined (insignificantly), there is a tendency

413 towards increasing frequency of both dry (T-only) and humid (T-and-T_E) heat wave days. In
414 regions characterized by large increases in HWD frequency, there is also a tendency toward
415 larger impacted areas. We also report changes in the magnitude of T and T_E when their
416 respective heat wave criteria are met. Our results show significant warming of T-only heat
417 waves in the SW region and significant increases in T_E during T-and-T_E heat waves in the MW
418 and NP regions.

419 Our findings are subject to several caveats. Our analysis is based on one observation-driven
420 data set (PRISM) and four reanalysis products that assimilate surface temperature and humidity
421 observations to varying degrees. However, the observational data set that is used here as a
422 reference is subject to uncertainties related to observations as well as methods (i.e.,
423 interpolation). As noted by Daly (2006), the true errors associated with gridded climate data are
424 largely unknown because the true underlying field is unknown. Nevertheless, PRISM has been
425 shown by Daly et al. (2008) to have smaller errors than other gridded products based on station
426 data, largely because of improved consideration of physiographic features in the interpolation
427 process. Because none of the reanalyses exhibit perfect agreement with PRISM across metrics,
428 our findings are contextualized by considering results from all of the products considered. The
429 general agreement among the results from different reanalysis suggests that our findings are
430 robust. For example, none of the data products considered here have significant trends of
431 opposing sign for any region and any metric in Tables 2-4. For approximately 60% of the trend
432 tests conducted, PRISM and the four reanalyses agree on the sign of the regional trend, but differ
433 in terms of the magnitude and statistical significance of the reported change. This finding is
434 consistent with the work on CONUS temperature trends by Vose et al., (2012) and regional
435 assessment of reanalysis-derived trends in summer temperature and precipitation by Bosilovich

436 (2013). Nevertheless, development of high resolution reference datasets for a range of variables
437 should continue to be a key goal for improved validation of reanalysis products.

438 Here, we have reported regional trends in T and T_E and their associated heat wave related
439 metrics, but largely avoided attribution of significant trends to specific drivers beyond the cross-
440 correlation and autocorrelation of temperature and humidity. In the case of heat waves, these
441 drivers are likely to occur across a range of spatial and temporal scales as described in the
442 introduction. Grotjahn et al. (2016) describe methods for identifying and characterizing large-
443 scale meteorological processes associated with extreme temperatures including large scale modes
444 of climate variability and communication of those variations to the regional scale. For example,
445 the positive tendencies in time series of T-only heat wave frequency and magnitude, coupled
446 with negative trends in specific humidity in the SW region, can be linked to broad regional
447 warming which may be attributable to observed widening of the tropics (Seidel et al. 2008),
448 while changes in other regions have been attributed to combinations of natural variability (e.g.,
449 Johnstone and Mantua, 2014) and radiative forcing from greenhouse gases.

450 Recent work indicates that regional forcing can also play an important role in the evolution
451 of the joint distribution of temperature and humidity. A lack of warming in parts of the NP and
452 MW regions is consistent with the observed "warming hole", which has been attributed to
453 hydrologic feedback (Pan et al. 2004), aerosol forcing (Yu et al. 2014), and tropical Pacific
454 variability (Meehl et al. 2015). Pryor et al. (2016) have demonstrated that the role irrigation
455 plays in equivalent temperature variability depends strongly on the regional climate and land
456 cover. In an application to oppressive heat events in Illinois, Ford and Schoof (2017) identified
457 similar large-scale circulation during T-only and T-and-T_E events and an important role for
458 regional soil moisture and land-atmosphere interaction. Along with urban heat island effects,

similar drivers were reported in the analysis of the 1995 Midwest heat wave by Kunkel et al., (1996), but have not been widely adopted in studies about future heat wave vulnerability.

Our analysis has demonstrated robust increases in both temperature and equivalent temperature across most US regions in recent decades. In many cases, these changes are manifest as increases in the frequency and intensity of extreme heat events and, in one region, as differential changes in the frequency of heat waves characterized by low (T-only) and high (T-and-T_E) humidity. Given the importance of humidity in determining the impacts of extreme temperatures, our findings reflect an important step toward understanding the changing impacts of extreme heat events in US regions. Improved understanding of heat wave characteristics and their dependence on processes occurring across scales should be a key focus for reducing impacts associated with extreme heat.

Acknowledgements

This material is based upon work supported by the US National Science Foundation under grants 1339629, 1339655 and 1502400, and the US Department of Energy (DE-SC0016438). Any opinions, findings, and conclusions or recommendations expressed in this material are those of the authors and do not necessarily reflect the view of the National Science Foundation or Department of Energy. We would also like to acknowledge the constructive comments of three anonymous reviewers.

References Cited

480 Anderson, G.B., and M.L. Bell, 2011: Heat waves in the United States: mortality risk during heat
481 waves and effect modification by heat wave characteristics in 43 U.S. communities. *Environ.*
482 *Health Persp.*, **119**, 210-218, doi:10.1289/ehp.1002313.
483 Bolton, D., 1980: The computation of equivalent potential temperature. *Mon. Wea. Rev.*, **108**,
484 1046-1053, doi:10.1175/1520-0493(1980)108<1046:TCOEPT>2.0.CO;2.
485 Bosilovich, M.G., 2013: Regional climate and variability of NASA MERRA and recent
486 reanalyses: U.S. summertime precipitation and temperature. *J. Appl. Meteor. Climatol.*, **52**,
487 1939-1951, doi:10.1175/JAMC-D-12-0291.1.
488 Bosilovich, M.G., and Coauthors, 2015: MERRA-2: Initial evaluation of the climate. NASA
489 Technical Report Series on Global Modeling and Data Assimilation, Volume 43.
490 Brown, P.J., and A.T. DeGaetano, 2013: Trends in U.S. surface humidity, 1930-2010. *J. Appl.*
491 *Meteor. Climatol.*, **52**, 147-163, doi:10.1175/JAMC-D-12-035.1.
492 Collins, M., and Coauthors, 2013: Long-term climate change: projections, commitments, and
493 irreversibility. In: *Climate Change 2013: The Physical Scientific Basis. Contribution of*
494 *Working Group I to the Fifth Assessment Report of the Intergovernmental Panel on Climate*
495 *Change* [Stocker, T.F., Qin, D., Plattner, G.-K., Tignor, M., Allen, S.K., Boschung, J.,
496 Nauels, A., Xia, Y., Bex, V., and P.M. Midgley (eds)]. Cambridge University Press,
497 Cambridge, United Kingdom and New York, NY, USA.
498 Dai, A., 2006: Recent climatology, variability, and trends in global surface humidity. *J. Climate*
499 **19**, 3589-3606.
500 Daly, C., 2006: Guidelines for assessing the suitability of spatial climate data sets. *Int. J.*
501 *Climatol.* **26**, 707-721.

Daly, C., and Coauthors, 2008: Physiographically sensitive mapping of climatological temperature and precipitation across the conterminous United States. *Int. J. Climatol.* **28**, 2031-2064, doi:01.1002/joc.1688.

Davey, C.A., Pielke Sr., R.A., and K.P. Gallo, 2006: Differences between near-surface equivalent temperature and temperature trends for the Eastern United States: equivalent temperature as an alternative measure of heat content. *Glob. Planet. Chang.,* **54**, 19-32.

Davis, L.W., and P.J. Gertler, 2015: Contribution of air conditioning adoption to future energy use under global warming. *P. Natl. Acad. Sci. USA*, **112**, 5962-5967, doi:10.1073/pnas.1423558112.

Dee, D.P., and Coauthors, 2011: The ERA-Interim reanalysis: configuration and performance of the data assimilation system. *Q. J. Roy. Meteor. Soc.,* **137**, 553-597, doi:10.1002/qj.828.

Fall, S., Diffenbaugh, N.S., Niyogi, D., Pielke Sr., R.A., and G. Rochon, 2010: Temperature and equivalent temperature over the United States (1979-2005). *Int. J. Climatol.,* **30**, 2045-2054, doi:10.1002/joc.2094.

Ford, T.W., and J.T. Schoof, 2016: Oppressive heat events in Illinois related to antecedent wet soils. *J. Hydrometeorol.,* **17**, 2713-2726, doi:10.1175/JHM-D-16.0075.1.

Ford, T.W., and J.T. Schoof, 2017: Characterizing extreme and oppressive heat waves in Illinois. *J. Geophys Res.-Atmos.*, **122**, 682-298, doi:10.1002/2016JD025721[.

Gaffen, D.J., and R.J. Ross, 1998: Increased summertime heat stress in the U.S. *Nature*, **396**, 529-530, doi:10.1038/25030.

Gaffen, D.J., and R.J. Ross, 1999: Climatology and trends in U.S. surface humidity and temperature. *J. Climate*, **12**, 811-828.

524 Grotjahn, R., and Coauthors, 2016: North American extreme temperature events and related
525 large scale meteorological patterns: a review of statistical methods, dynamics, modeling, and
526 trends. *Clim. Dynam.*, **46**, 1151-1184, doi:10.1007/s00382-015-2638-6.
527 Grundstein, A., and J. Dowd, 2011: Trends in extreme apparent temperatures over the United
528 States, 1949-2010. *J. Appl. Meteor. Climatol.*, **50**, 1650-1653, doi:10.1175/JAMC-D-11-
529 063.1.
530 Held, I.M., and B.J. Soden, 2006: Robust response of the hydrologic cycle to global warming. *J.*
531 *Climate* **19**, 5686-5699.
532 Hoerling, M., and Coauthors, 2013: Anatomy of an extreme event. *J. Climate*, **26**, 2811-2832,
533 doi:10.1175/JCLI-D-12-00270.1.
534 Hondula, D.M., Balling Jr., R.C., Vanos, J.K., and M. Georgescu, 2015: Rising temperatures,
535 human health, and the role of adaptation. *Curr. Clim. Change Rep.*, **1**, 144-154,
536 doi:10.1007/s40641-015-0016-4.
537 Johnstone, J.A., and N.J. Mantua, 2014: Atmospheric controls on northeast Pacific temperature
538 variability and change, 1900-2012. *Proc. Natl. Acad. Sci. U.S.A.* **111**, 14360-14365,
539 doi:10.1073/pnas.1318371111.
540
541 Kobayashi, S., and Coauthors, 2015: The JRA-55 reanalysis: general specifications and basic
542 characteristics. *J. Meteorol. Soc. Jpn.*, **93**, 5-48, doi:10.2151/jmsj.2015-001.
543 Kravchenko, J., Abernethy, A.P., Fawzy, M., and H.K. Lyerly, 2013: Minimization of heatwave
544 morbidity and mortality. *Am. J. Prev. Med.*, **44**, 274-282.

545 Kunkel, K.E., Changnon, S.A., Reinke, B.C., and R.W. Arritt, 1996: The July 1995 heat wave in
546 the Midwest: A climatic perspective and critical weather factors. *B. Am. Meteorol. Soc.,* **77**,
547 1507-1518, doi:10.1175/1520-0477(1996)077<1507:TJHWIT>2.0.CO;2
548 Lanzante, J.R., 1996: Resistant, robust and non-parametric techniques for the analysis of climate
549 data: theory and examples, including applications to historical radiosonde station data. *Int. J.*
550 *Climatol.*, **16**, 1197-1226, doi:10.1002/(SICI)1097-0088(199611)16:11<1197::AID-
551 JOC89>3.0.CO;2-L.
552 Lobell, D.B., Roberts, M.J., Schlenker, W., Braun, N., Little, B.B., Rejesus, R.M., and G.L.
553 Hammer, 2014: Greater sensitivity to drought accompanies maize yield increase in the U.S.
554 Midwest. *Science* **344**, 516-519.
555 MacDonald, G.M., 2010. Water, climate change, and sustainability in the southwest. *Proc. Natl.*
556 *Acad. Sci. U.S.A.* **107**, 21256-21262, doi:10.1073/pnas.0909651107.
557 Meehl, G.A., J.M. Arblaster, and C.T.Y. Chung, 2015: Disappearance of the southeast U.S.
558 "warming hole" with the late 1990s transition of the Interdecadal Pacific Oscillation.
559 *Geophys. Res. Lett.*, **42**, 5564-5570, doi:10.1002/2015GL064586.
560 Melillo, J.M., Richmond, T.C., and G.W. Yohe (Eds), 2014: *Climate Change Impacts in the*
561 *United States: The Third National Climate Assessment*, U.S. Global Change Research
562 Program, 841 pp, doi:10.7930/J0Z31WJ2.
563 Mesinger, F., and Coauthors, 2006: North American regional reanalysis. *B. Am. Meteorol. Soc.*
564 **87**, 343-360, doi:10.1175/BAMS-87-3-343.
565 Metzger, K.B., Ito, K., and T.D. Matte, 2010: Summer heat and mortality in New York City:
566 How hot is too hot? *Environ. Health Persp.,* **118**, 80-86, doi:10.1289/ehp.0900906.

567 Miller, N.L., Hayhoe, K., Jin, J., and M. Auffhammer, 2008: Climate, extreme heat, and
568 electricity demand in California. *J. Appl. Meteor. Climatol.,* **47**, 1834-1844,
569 doi:10.1175/2007JAMC1480.1.
570 Mishra, V., and K.A. Cherkauer, 2010: Retrospective droughts in the crop growing season:
571 implications to corn and soybean yield in the Midwestern United States. *Agr. Forest*
572 *Meteorol.,* **150**, 1030-1045, doi:10.1016/j.agrformet.2010.04.002.
573 NWS, 2016: 76-year list of severe weather fatalities. [Available online at
574 http://www.nws.noaa.gov/om/hazstats/resources/weather_fatalities.pdf]
575 Pan, Z., R.W. Arritt, E.S. Takle, W.J. Gutowski, C.J. Anderson, and M. Segal, 2004: Altered
576 hydrologic feedback in a warming climate introduces a "warming hole". *Geophys. Res. Lett.*,
577 **31**, L17109, doi:10.1029/2004GL020528.
578 Pielke Sr., R.A., Davey, C., and J. Morgan, 2004: Assessing "global warming" with surface heat
579 content. *EOS: Trans. Am. Geophys. Union,* **85**, 210-211, doi:10.1029/2004EO210004.
580 Pryor, S.C., and J.T. Schoof, 2016: Evaluation of near-surface temperature, humidity and
581 equivalent temperature from Regional Climate Models applied in type-II downscaling. *J.*
582 *Geophys Res.-Atmos.* **121** doi: 10.1002/2015JD024539.
583 Pryor, S.C., Sullivan, R.C., and T. Wright, 2016: Quantifying the roles of changing albedo,
584 emissivity, and energy partitioning in the impact of irrigation on atmospheric heat content. *J.*
585 *Appl. Meteor. Climatol.* **55**, 1699-1706, doi:10.1175/JAMC-D-15-0291.1.
586 Schoof, J.T., Heern, Z.A., Therrell, M.D., and J.W.F. Remo, 2015: Assessing trends in lower
587 tropospheric heat content in the central United States using equivalent temperature. *Int. J.*
588 *Climatol.*, **35**, 2828-2836, doi:10.1002/joc.4175.

589 Seager, R., Naik, N., and L. Vogel, 2012: Does global warming cause intensified interannual
590 hydroclimate variability? *J. Climate,* **25**, 3355-3372, doi:10.1175/JCLI-D-11-00363.1.
591 Seidel, D.J., Q. Fu, W.J. Randel, and T.J. Reichler, 2008: Widening of the tropical belt in a
592 changing climate. *Nat. Geosci.*, **1**, 21-24, doi:10.1038/ngeo.2007.38.
593 Sen, P.K., 1968: Estimates of the regression coefficient based on Kendall's Tau. *J. Am. Stat.*
594 *Assoc.,* **63**, 1379-1389, doi:10.1080/01621459.1968.10480934.
595 Seneviratne, S.I., Donat, M.G., Mueller, B., and L.V. Alexander, 2014: No pause in the increase
596 of hot temperature extremes. *Nat. Clim. Chang.*, **4**, 161-163, doi:10.1038/nclimate2145.
597 Souch, C., and C.S.B. Grimmond, 2004: Applied climatology: 'heat waves'. *Prog. Phys. Geogr.*.
598 **28**, 599-606, doi:10.1191/0309133304pp428pr.
599 Steadman, R.G., 1984: A universal scale of apparent temperature. *J. Clim. Appl. Meteorol.*, **23**,
600 1674-1687, doi:10.1175/1520-0450(1984)023<1674:AUSOAT>2.0.CO;2.
601 Taylor, K.E., 2001: Summarizing multiple aspects of model performance in a single diagram. *J.*
602 *Geophys Res.-Atmos.*, **106**, 7183-7192, doi:10.1029/2000JD900719.
603 Trenberth, K.E., and G.W. Branstator, 1992: Issues in establishing causes of the 1998 drought
604 over North America. *J. Climate,* **5**, 159-172, doi:10.1175/1520-
605 0442(1992)005<0159:IIECOT>2.0.CO;2.
606 Vose, R.S., Applequist, S., Menne, M.J., Williams Jr., C.N., and P. Thorne, 2012: An
607 Intercomparison of temperature trends in the U.S. Historical Climatology Network and recent
608 atmospheric reanalyses. *Geophys. Res. Lett.*, **39**, L10703, doi:10.1029/2012GL051387.
609 Yu, S., K. Alapaty, R. Mathur, J. Pleim, Y. Zhang, C. Nolte, B. Eder, K. Foley, and T.
610 Nagashima, 2014: Attribution of the United States "warming hole": Aerosol indirect effect
611 and precipitable water vapor. *Scientific Reports,* **4**, doi:10.1038/srep06929.

612 **Figure captions**

613 **Figure 1.** Map of study area showing regions: Northeast (NE), Southeast (SE), Midwest (MW),
614 Northern Plains (NP), Southern Plains (SP), Southwest (SW) and Northwest (NW).

615

616 **Figure 2**. Maps, Taylor diagrams, and regional averages of summer (JJA) mean (a, e, i; °C),
617 standard deviation (b, f, j; °C), interannual variability (c, g, k; °C), and 35-year linear trend (d, h,
618 l; °C decade^{-1}) of 2-m air temperature. The maps show the results from the PRISM data set. The
619 Taylor diagrams show the correlation between the PRISM field and each reanalysis field (on the
620 radial axis), the spatial standard deviation (on the x- and y-axes) and the pattern-centered RMSE
621 (on the circular axis). The data sets shown are PRISM (P), ERA-Interim (E), JRA-55 (J),
622 MERRA-2 (M), and NARR (N).

623

624 **Figure 3**. Maps, Taylor diagrams, and regional averages of summer (JJA) mean (a, e, i; g kg^{-1}),
625 standard deviation (b, f, j; g kg^{-1}), interannual variability (c, g, k; g kg^{-1}), and 35-year linear trend
626 (d, h, l; g kg^{-1} decade^{-1}) of 2-m specific humidity (q). The maps show the results from the
627 PRISM data set. The Taylor diagrams show the correlation between the PRISM field and each
628 reanalysis field (on the radial axis), the spatial standard deviation (on the x- and y-axes) and the
629 pattern-centered RMSE (on the circular axis). The data sets shown are PRISM (P), ERA-Interim
630 (E), JRA-55 (J), MERRA-2 (M), and NARR (N).

631

632 **Figure 4**. Maps, Taylor diagrams, and regional averages of summer (JJA) mean (a, e, i; °C),
633 standard deviation (b, f, j; °C), interannual variability (c, g, k; °C), and 35-year linear trend (d, h,
634 l; °C decade^{-1}) of 2-m equivalent temperature (T_E). The maps show the results from the PRISM

635 data set. The Taylor diagrams show the correlation between the PRISM field and each reanalysis
636 field (on the radial axis), the spatial standard deviation (on the x- and y-axes) and the pattern-
637 centered RMSE (on the circular axis). The data sets shown are PRISM (P), ERA-Interim (E),
638 JRA-55 (J), MERRA-2 (M), and NARR (N).
639
640 **Figure 5.** Mean annual heat wave day (HWD) frequency and magnitude by region. Results are
641 shown for the PRISM data set (gray bars) as well as the ERA-Interim (■), JRA-55 (●), MERRA-
642 2 (♦) and NARR (▼) reanalysis products. The frequency of T-only and T-and-T_E HWDs are
643 shown in panels a) and b), respectively. Panel c shows the mean magnitude (see Section 3.2) of
644 T on T-only HWDs. The mean magnitudes of T and T_E on T-and-TE HWDs are shown in panels
645 d) and e), respectively.
646
647 **Figure 6**. Time series of summer (JJA) heat wave day (HWD) frequency (days/year) for U.S.
648 regions (as in Figure 1) based on the PRISM data set. For each subplot, time series are presented
649 for T-only HWDs (circle with solid line marker) and T-and-T_E HWDs (square with dotted line
650 marker). Time series with significant linear trends (with α=0.10, see Section 3) are indicated
651 with filled symbols and an added trend line. Numerical values of the trends are provided in
652 Table 2.
653
654 **Figure 7.** Scatter diagrams exhibiting the relationships between the Spearman correlation of
655 daily T and q and a) the frequency of T-and-T_E HWDs and b) the mean T_E magnitude (as defined
656 in Section 3) on T-and-T_E HWDs.
657

Figure 8: Time series of mean regional proportion impacted by heat wave conditions (proportion/year) for U.S. regions (as in Figure 1) based on the PRISM data set. For each subplot, time series are presented for T-only HWDs (circle with solid line marker) and T-and-T_E HWDs (square with dotted line marker). Time series with significant linear trends (with α=0.10) are indicated with filled symbols and an added trend line. Numerical values of the trends are provided in Table 3.

Figure 9: Time series of mean heat wave magnitude for U.S. regions (as in Figure 1) based on the PRISM data set. For each subplot, time series are presented for T on T-only HWDs (circle with solid line marker) and T-and-T_E HWDs (square with dotted line marker) and T_E on T-and-T_E HWDs (diamond with dotted line marker). Time series with significant linear trends (with α=0.10) are indicated with filled symbols and an added trend line. Numerical values of the trends are provided in Table 4.

672 **Table 1.** General characteristics of data sets used in this study.

Institute	Data Product	Spatial Res.	Assimil. of 2-m T	Assimil. of 2-m q	Reference
PRISM Climate Group, Oregon State University	PRISM	~4 km	N/A	N/A	Daly et al. (2008)
European Center for Medium-Range Weather Forecasting (ECMWF)	ERA-Interim Reanalysis (ERA-Interim)	0.75°	Yes	Yes	Dee et al. (2011)
Japanese Meteorological Agency(JMA)	JRA-55 Year Reanalysis (JRA-55)	1.25°	Yes	Yes	Kobayashi et al. (2015)
National Aeronautics and Space Administration (NASA)	MERRA-2 Reanalysis (MERRA-2)	0.625°	No	No	Bosilovich et al. (2015)
National Centers for Environmental Prediction (NCEP)	North American Regional Reanalysis (NARR)	~32 km	No	Yes	Mesinger et al. (2006)

673

674

675 **Table 2**. Linear trends in the number of heat wave days (HWDs; n/decade) for T-only and T-

676 and-T_E heat wave types. Bold trends indicate significance with α=0.10.

T-only HWDs	NE	SE	MW	NP	SP	SW	NW
PRISM	0.06	0.35	0.03	-0.04	**0.99**	**1.34**	**0.55**
ERA-Interim	0.10	**0.72**	0.09	-0.11	**1.29**	**1.43**	**0.50**
JRA-55	0.03	**0.64**	0.10	-0.05	**1.14**	**1.25**	**0.71**
MERRA-2	0.04	0.23	0.08	-0.13	**1.02**	**0.82**	0.25
NARR	0.04	0.31	0.16	-0.05	**1.01**	**1.01**	0.15
T-and-T_E HWDs	NE	SE	MW	NP	SP	SW	NW
PRISM	0.59	0.34	0.29	0.12	**0.13**	0.20	0.43
ERA-Interim	0.47	0.23	0.38	0.04	**0.09**	0.13	**0.65**
JRA-55	0.21	0.18	0.32	0.22	**0.15**	0.18	**0.56**
MERRA-2	**0.88**	**0.35**	**0.58**	0.23	**0.11**	**0.47**	0.50
NARR	**0.78**	**0.47**	**0.57**	0.00	**0.11**	0.08	0.17

677

678 **Table 3**. Linear trends in the mean and maximum regional areal proportions (%/decade) of
679 regional area impacted by heat wave conditions for T-only and T-and-T_E heat wave types. Bold
680 trends indicate significance with α=0.10.

Mean Areal Proportion: T-only HWDs	NE	SE	MW	NP	SP	SW	NW
PRISM	0.08	0.17	-0.01	-0.34	**1.09**	**1.53**	**1.00**
ERA-Interim	-0.06	0.76	0.11	-0.47	**2.06**	**1.65**	**1.22**
JRA-55	0.23	0.89	0.59	-0.84	**1.52**	**1.44**	**1.73**
MERRA-2	-0.13	0.12	-0.14	-0.92	1.43	0.94	0.80
NARR	-0.21	0.39	0.21	-0.44	0.95	**1.05**	0.69
Mean Areal Proportion: T-and-T_E HWDs	NE	SE	MW	NP	SP	SW	NW
PRISM	0.44	0.26	0.68	0.07	0.19	0.18	1.02
ERA-Interim	1.45	0.21	-0.03	-0.14	0.40	0.24	1.83
JRA-55	0.00	0.46	1.17	0.62	0.06	0.06	1.69
MERRA-2	**2.73**	0.62	**1.22**	1.07	**0.41**	**0.57**	1.96
NARR	0.31	0.74	**1.45**	-0.05	**0.35**	-0.03	0.85
Maximum Areal Proportion: T-only HWDs	NE	SE	MW	NP	SP	SW	NW
PRISM	1.21	1.41	-1.02	-2.64	**8.20**	**6.80**	**5.74**
ERA-Interim	1.09	3.49	1.42	-2.29	**12.15**	**9.22**	**6.96**
JRA-55	1.21	4.58	1.51	-0.92	**7.14**	**8.26**	**7.27**
MERRA-2	0.00	1.17	-0.10	-3.48	**8.04**	**4.96**	2.73
NARR	0.39	2.80	1.31	-2.06	**7.26**	**7.50**	2.38
Maximum Areal Proportion: T-and-T_E HWDs	NE	SE	MW	NP	SP	SW	NW
PRISM	7.72	4.86	3.30	1.18	1.67	2.53	4.40
ERA-Interim	6.54	4.37	1.31	-0.78	**2.00**	2.92	**6.88**
JRA-55	1.68	3.81	3.71	1.47	1.10	2.53	4.44
MERRA-2	**11.87**	**6.64**	**7.19**	1.44	**2.21**	**4.75**	4.95
NARR	**7.68**	**6.51**	5.45	1.21	**1.89**	0.29	1.94

681

682

683 **Table 4**. Linear trends in the mean and maximum magnitude (°C/decade) of regional heat wave

684 conditions for T-only and T-and-T_E heat wave types. Bold trends indicate significance (α=0.10).

Mean T Magnitude: T-only HWDs	NE	SE	MW	NP	SP	SW	NW
PRISM	0.05	0.03	-0.04	0.00	0.03	**0.05**	**0.10**
ERA-Interim	-0.01	0.02	0.00	-0.06	-0.01	0.02	0.04
JRA-55	-0.01	0.06	-0.01	0.02	0.03	**0.13**	**0.09**
MERRA-2	-0.02	0.01	-0.04	-0.03	0.02	0.03	0.05
NARR	-0.05	0.04	0.05	0.00	0.01	0.03	0.06
Mean T Magnitude: T-and-T_E HWDs	NE	SE	MW	NP	SP	SW	NW
PRISM	0.01	0.01	-0.05	-0.04	-0.01	-0.01	0.03
ERA-Interim	0.01	0.02	-0.03	-0.04	-0.02	0.04	0.13
JRA-55	-0.04	-0.01	-0.03	-0.06	0.01	-0.02	0.08
MERRA-2	-0.05	-0.05	-0.01	-0.04	0.00	**-0.07**	0.02
NARR	-0.02	0.04	-0.03	0.03	0.04	-0.02	0.04
Mean T_E Magnitude: T-and-T_E HWDs	NE	SE	MW	NP	SP	SW	NW
PRISM	0.12	0.07	**0.30**	**0.26**	0.08	-0.10	-0.02
ERA-Interim	0.22	-0.11	0.01	0.04	-0.01	**-0.18**	-0.08
JRA-55	0.08	-0.06	0.18	**0.30**	-0.01	**-0.19**	-0.12
MERRA-2	**0.20**	0.06	0.09	**0.32**	0.09	-0.04	**-0.16**
NARR	**0.27**	**0.16**	**0.34**	**0.23**	**0.15**	-0.04	0.06
Maximum T Magnitude: T-only HWDs	NE	SE	MW	NP	SP	SW	NW
PRISM	**0.24**	**0.16**	-0.22	0.01	0.06	-0.07	**0.36**
ERA-Interim	0.10	0.05	0.08	-0.17	-0.07	0.06	**0.31**
JRA-55	0.03	0.16	-0.17	0.08	0.16	**0.33**	0.27
MERRA-2	0.09	**0.08**	0.04	-0.07	0.14	0.00	0.24
NARR	-0.13	0.20	0.33	-0.07	0.09	0.04	0.03
Maximum T Magnitude: T-and-T_E HWDs	NE	SE	MW	NP	SP	SW	NW
PRISM	**0.23**	0.06	0.01	0.15	-0.01	0.03	**0.46**
ERA-Interim	0.11	0.04	-0.01	-0.07	0.07	0.27	0.28
JRA-55	0.06	-0.03	-0.03	-0.12	0.13	0.17	0.20
MERRA-2	0.07	0.00	0.01	-0.04	0.14	0.05	0.01
NARR	0.11	0.08	0.15	0.00	0.05	-0.01	-0.01
Maximum T_E Magnitude: T-and-T_E HWDs	NE	SE	MW	NP	SP	SW	NW
PRISM	**0.56**	**0.47**	**1.15**	**1.03**	0.42	0.16	-0.28
ERA-Interim	**0.53**	-0.12	**0.84**	0.08	0.32	0.01	0.11
JRA-55	0.18	-0.27	**0.71**	**0.69**	0.37	0.09	0.13
MERRA-2	0.37	0.37	-0.17	0.62	**0.46**	0.27	-0.13
NARR	**0.85**	**0.44**	0.43	**1.04**	**0.60**	-0.14	0.21

685

686

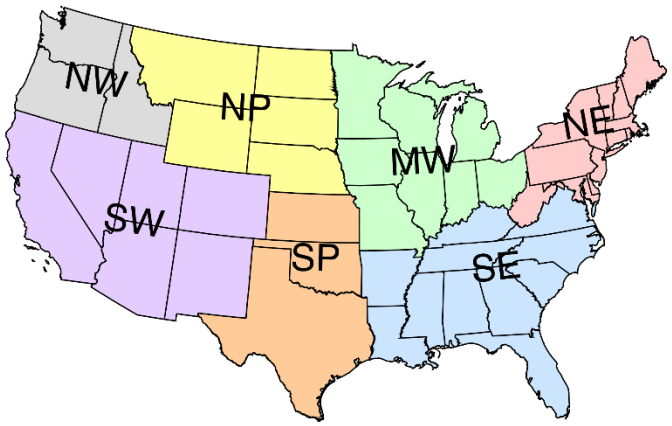

687

688 **Figure 1.** Map of study area showing regions: Northeast (NE), Southeast (SE), Midwest (MW),

689 Northern Plains (NP), Southern Plains (SP), Southwest (SW) and Northwest (NW).

690

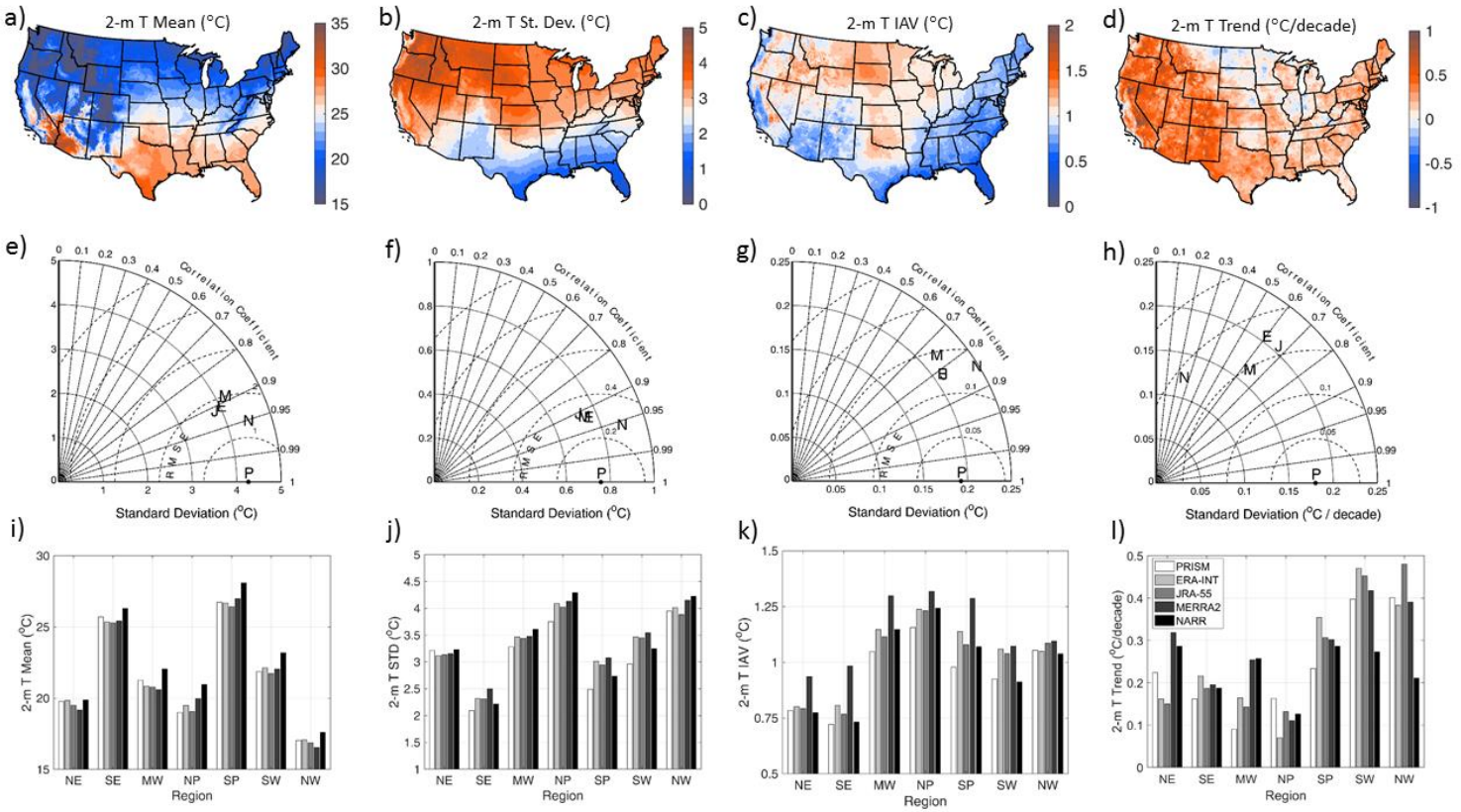

Figure 2. Maps, Taylor diagrams, and regional averages of summer (JJA) mean (a, e, i; °C), standard deviation (b, f, j; °C), interannual variability (c, g, k; °C), and 35-year linear trend (d, h, l; °C decade^{-1}) of 2-m air temperature. The maps show the results from the PRISM data set. The Taylor diagrams show the correlation between the PRISM field and each reanalysis field (on the radial axis), the spatial standard deviation (on the x- and y-axes) and the pattern-centered RMSE (on the circular axis). The data sets shown are PRISM (P), ERA-Interim (E), JRA-55 (J), MERRA-2 (M), and NARR (N).

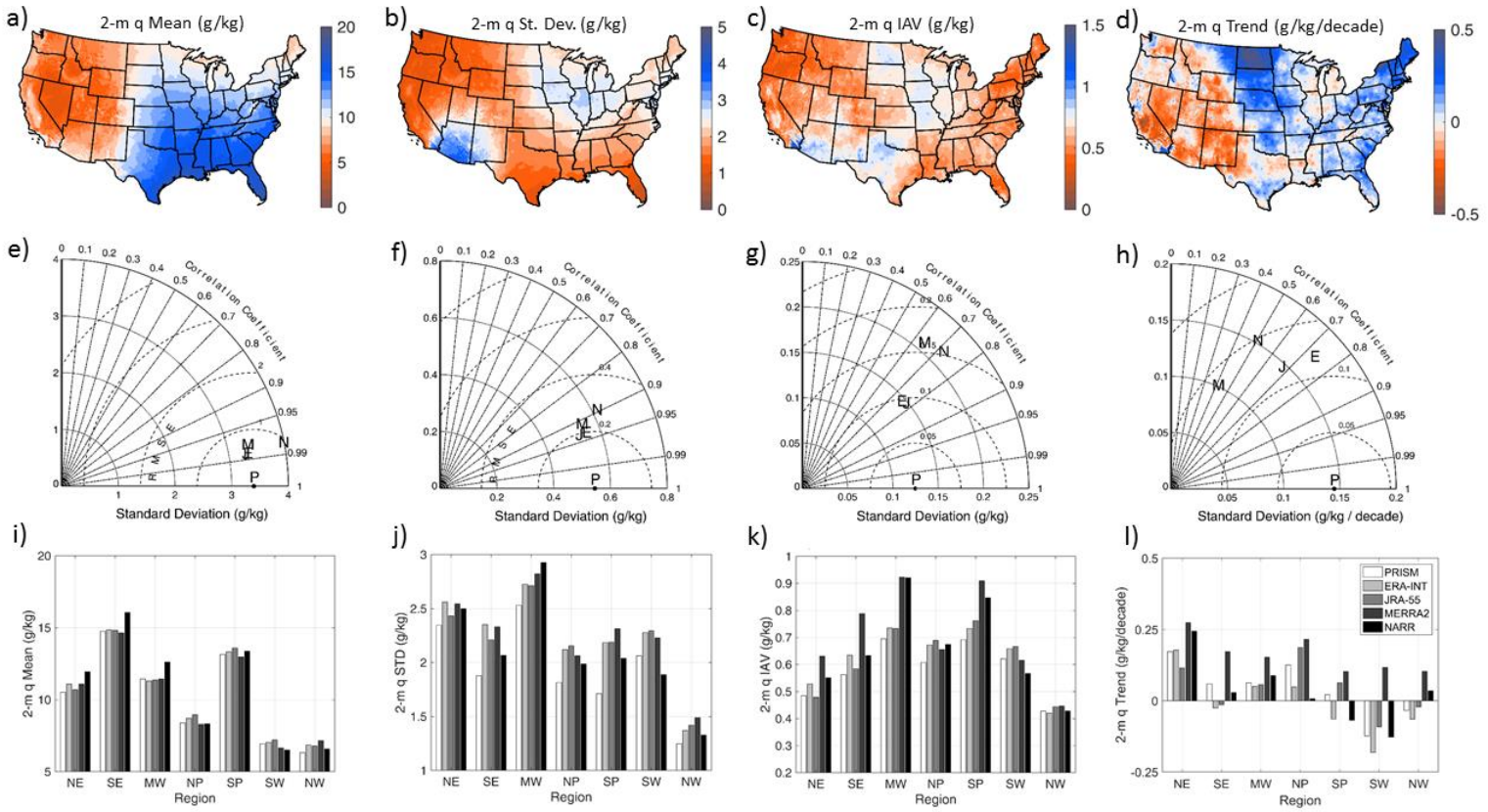

Figure 3. Maps, Taylor diagrams, and regional averages of summer (JJA) mean (a, e, i; g kg^{-1}), standard deviation (b, f, j; g kg^{-1}), interannual variability (c, g, k; g kg^{-1}), and 35-year linear trend (d, h, l; g kg^{-1} decade^{-1}) of 2-m specific humidity (q). The maps show the results from the PRISM data set. The Taylor diagrams show the correlation between the PRISM field and each reanalysis field (on the radial axis), the spatial standard deviation (on the x- and y-axes) and the pattern-centered RMSE (on the circular axis). The data sets shown are PRISM (P), ERA-Interim (E), JRA-55 (J), MERRA-2 (M), and NARR (N).

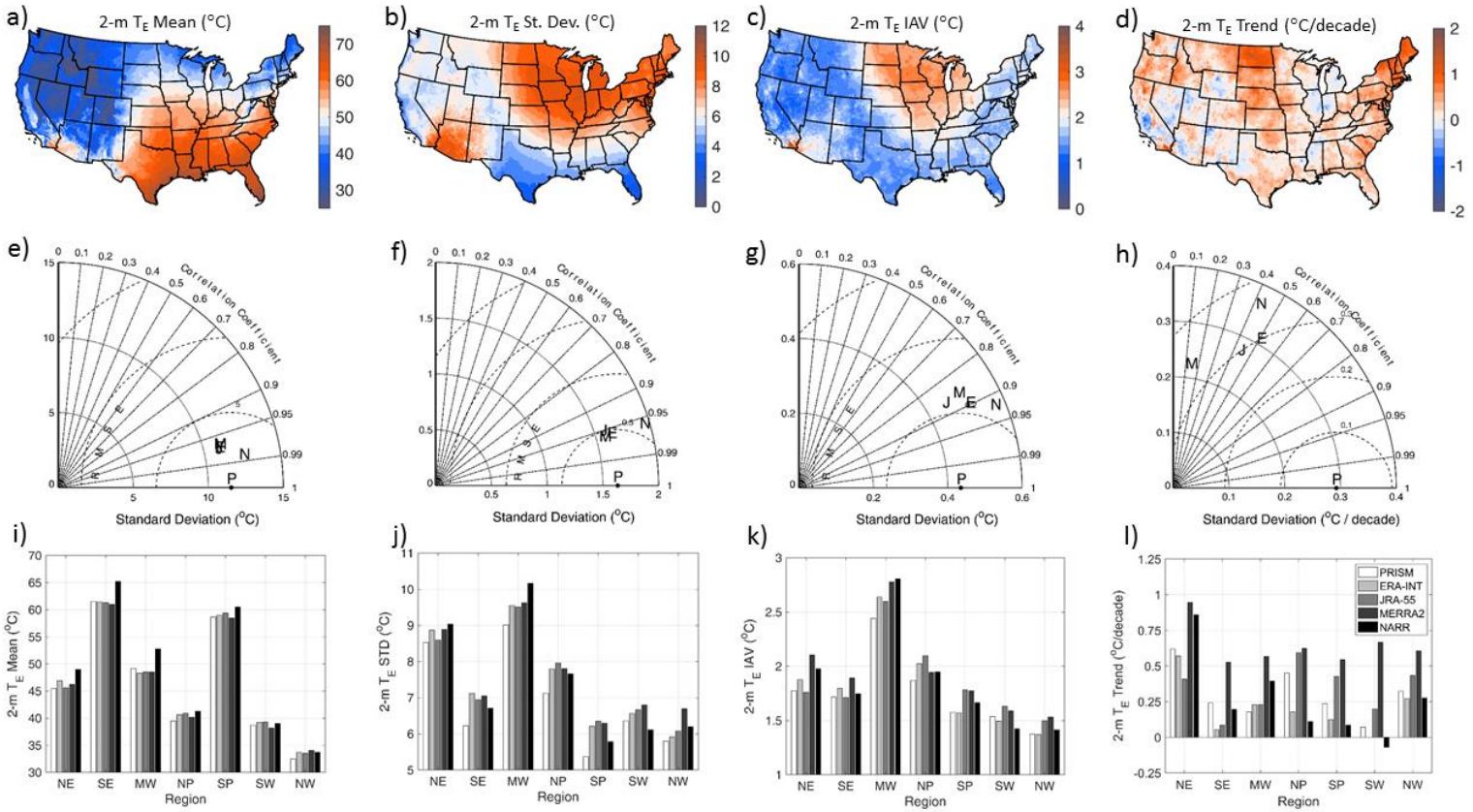

Figure 4. Maps, Taylor diagrams, and regional averages of summer (JJA) mean (a, e, i; °C), standard deviation (b, f, j; °C), interannual variability (c, g, k; °C), and 35-year linear trend (d, h, l; °C decade^{-1}) of 2-m equivalent temperature (T_E). The maps show the results from the PRISM data set. The Taylor diagrams show the correlation between the PRISM field and each reanalysis field (on the radial axis), the spatial standard deviation (on the x- and y-axes) and the pattern-centered RMSE (on the circular axis). The data sets shown are PRISM (P), ERA-Interim (E), JRA-55 (J), MERRA-2 (M), and NARR (N).

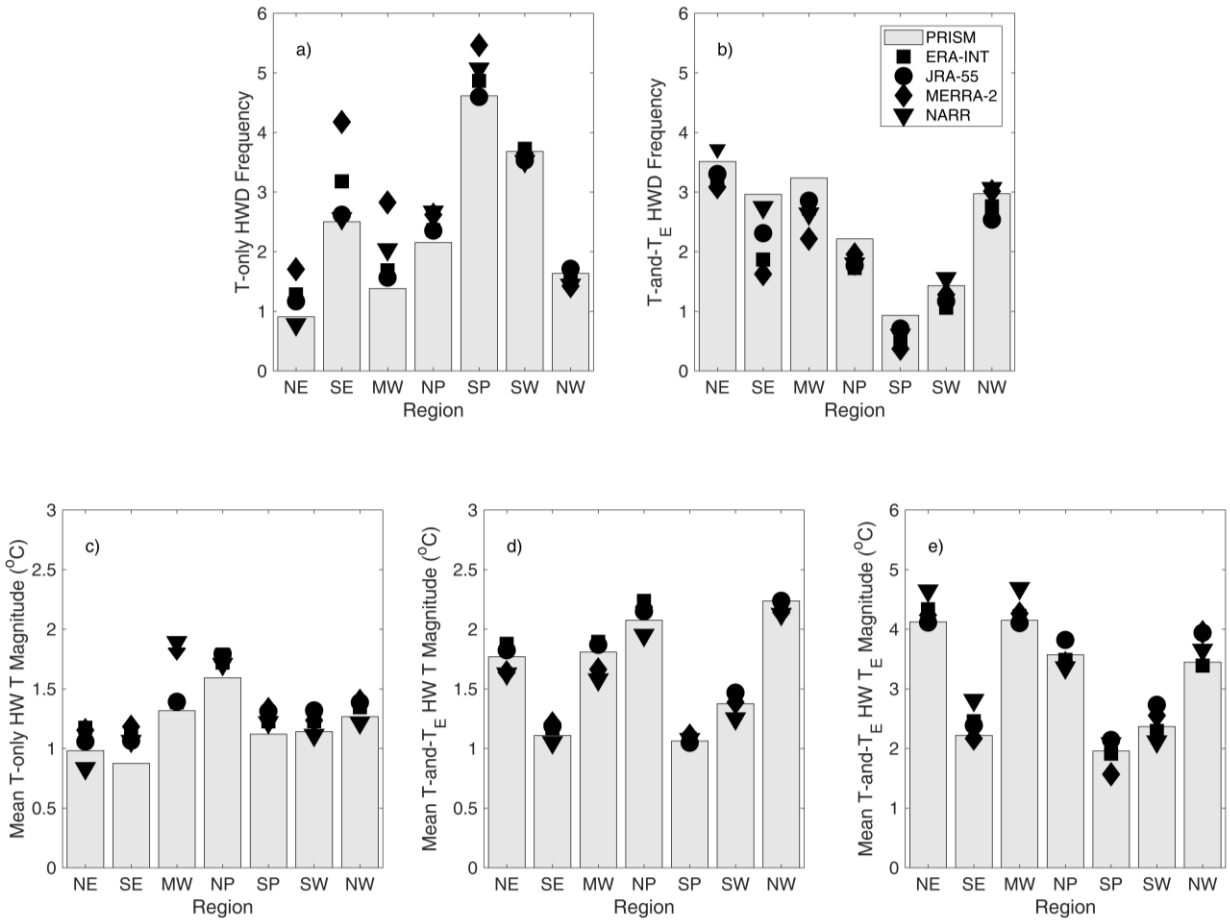

709

710 **Figure 5.** Mean annual heat wave day (HWD) frequency and magnitude by region. Results are
711 shown for the PRISM data set (gray bars) as well as the ERA-Interim (■), JRA-55 (●), MERRA-
712 2 (♦) and NARR (▼) reanalysis products. The frequency of T-only and T-and-T_E HWDs are
713 shown in panels a) and b), respectively. Panel c shows the mean magnitude (see Section 3.2) of
714 T on T-only HWDs. The mean magnitudes of T and T_E on T-and-TE HWDs are shown in panels
715 d) and e), respectively.

716

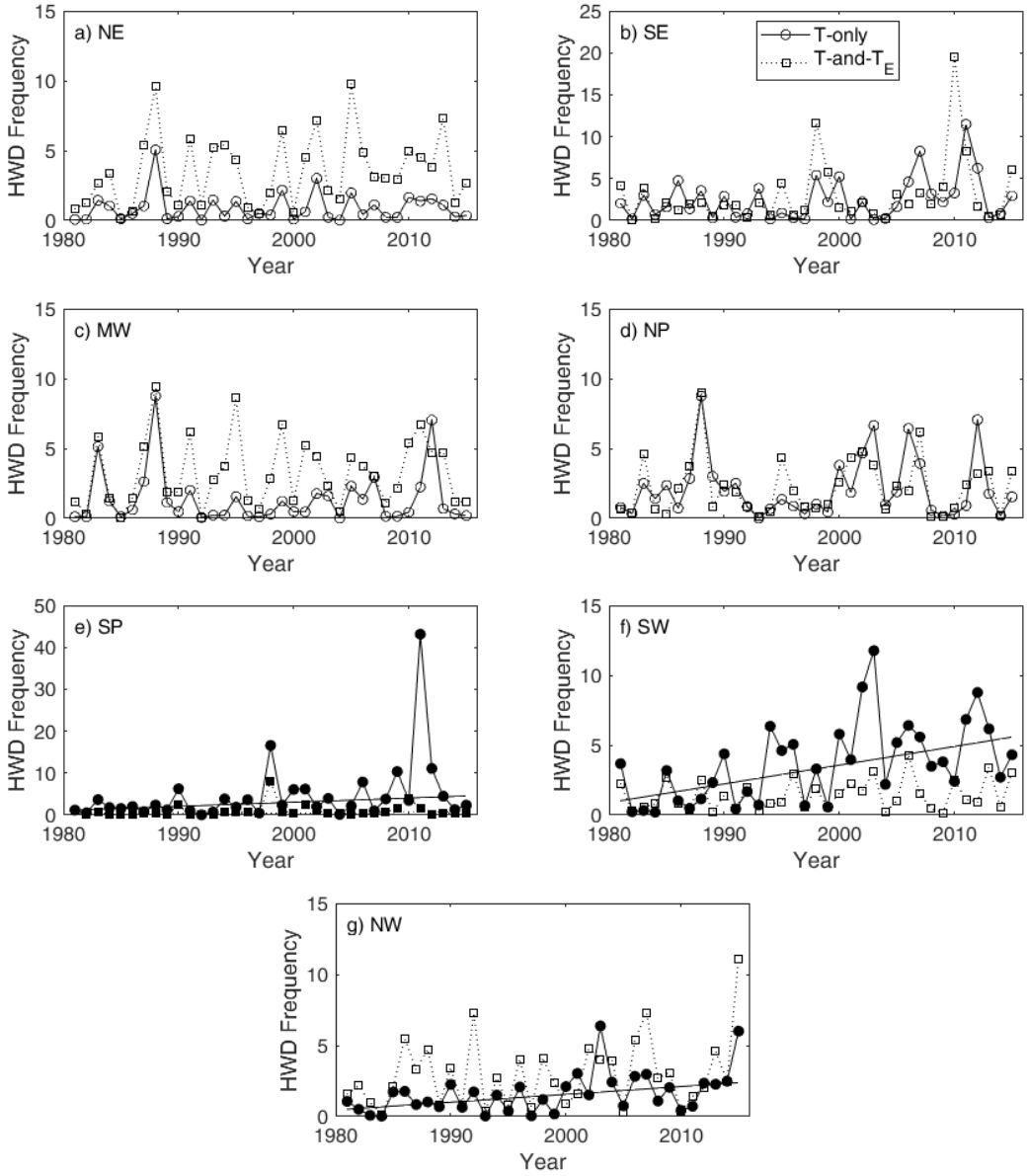

717

718 **Figure 6**. Time series of summer (JJA) heat wave day (HWD) frequency (days/year) for U.S.
719 regions (as in Figure 1) based on the PRISM data set. For each subplot, time series are presented
720 for T-only HWDs (circle with solid line marker) and T-and-T_E HWDs (square with dotted line
721 marker). Time series with significant linear trends (with α=0.10, see Section 3) are indicated
722 with filled symbols and an added trend line. Numerical values of the trends are provided in
723 Table 2.

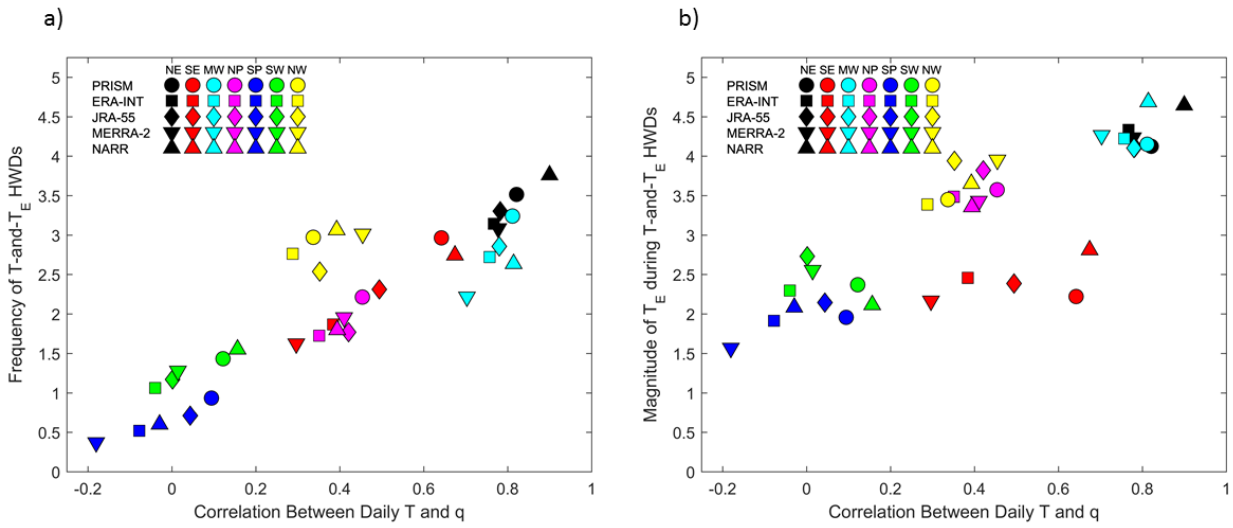

724

725 **Figure 7.** Scatter diagrams exhibiting the relationships between the Spearman correlation of

726 daily T and q and a) the frequency of T-and-T_E HWDs and b) the mean T_E magnitude (as defined

727 in Section 3) on T-and-T_E HWDs.

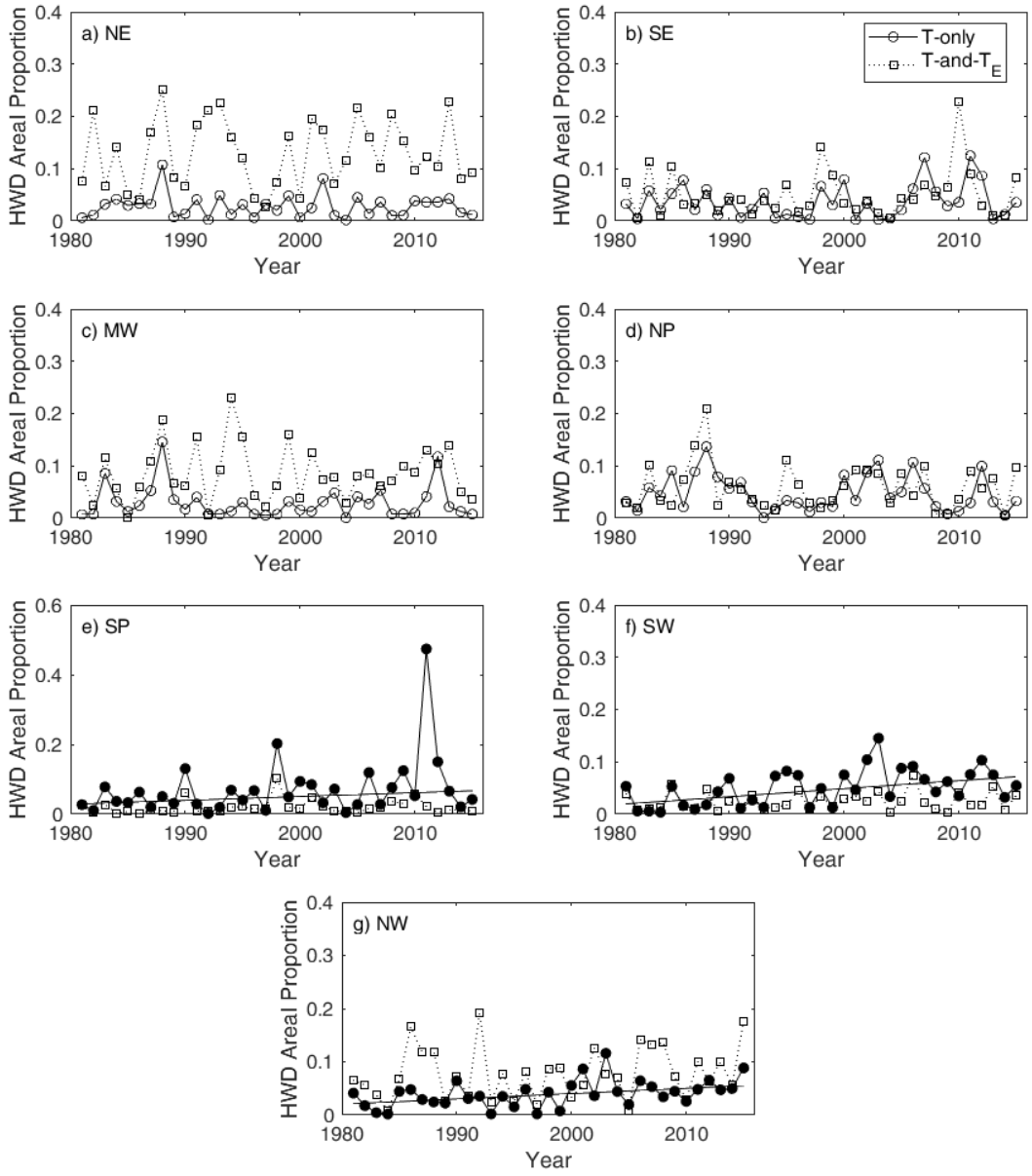

728

729 **Figure 8**: Time series of mean regional proportion impacted by heat wave conditions
730 (proportion/year) for U.S. regions (as in Figure 1) based on the PRISM data set. For each
731 subplot, time series are presented for T-only HWDs (circle with solid line marker) and T-and-T_E
732 HWDs (square with dotted line marker). Time series with significant linear trends (with α=0.10)
733 are indicated with filled symbols and an added trend line. Numerical values of the trends are
734 provided in Table 3.

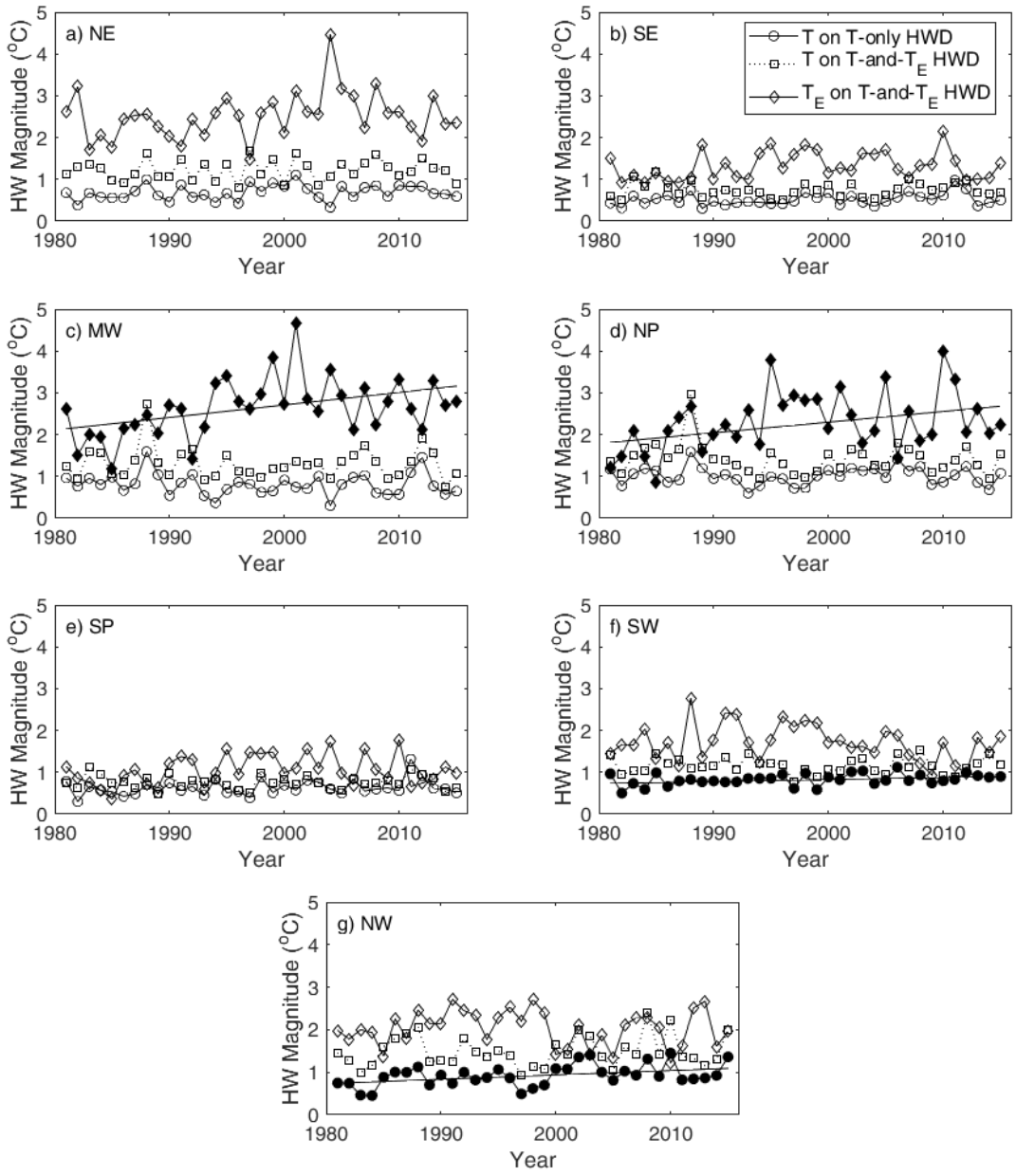

735

736 **Figure 9**: Time series of mean heat wave magnitude for U.S. regions (as in Figure 1) based on
737 the PRISM data set. For each subplot, time series are presented for T on T-only HWDs (circle
738 with solid line marker) and T-and-T_E HWDs (square with dotted line marker) and T_E on T-and-
739 T_E HWDs (diamond with dotted line marker). Time series with significant linear trends (with
740 α=0.10) are indicated with filled symbols and an added trend line. Numerical values of the
741 trends are provided in Table 4.